Orbiting phenomenon in ^{16}O-^{28}Si scattering

C. S. Shastry*
Groupe de Physique Nucléaire Théorique,
Centre de Recherches Nucléaires et U.L.P. Strasbourg, 67037 Strasbourg Cedex, France

I. Parija
Post Graduate Department of Physics, Sambalpur University, Jyoti Vihar, Burla, Orissa 768017, India
(Received 1 October 1982)

From an analysis of the effective potentials and the surface region behavior of quantum mechanical radial wave functions, we find that the most interesting physical phenomena taking place in $^{16}O+^{28}Si$ scattering at $E_{lab}=55$ MeV is the orbiting mechanism for $l=24$, 25, 26. We find that the orbital amplitude $A_0(\theta)$ generated by these partial waves acts coherently at large angles with the background amplitude $A_b(\theta)$ describing the remainder of the full amplitude. The enhanced large angle oscillations are caused by the almost, but not complete, destructive interference between $A_0(\theta)$ and $A_b(\theta)$. Using appropriate mathematical techniques, we show that at large angles $\theta \lesssim 180°$, both $A_0(\theta)$ and $A_b(\theta)$ are dominated essentially by the same Legendre polynomial. This explains the observation of Takemasa and Tamura that the cross sections generated by *exact* Regge pole terms behave quite similarly to that generated by the corresponding Regge background terms. Furthermore, our analysis clarifies the underlying reason for the success of the purely parametric Regge pole model at large angles. We also compare the infinite sequence of Regge poles generated by the barrier term in the Wentzel-Kramers-Brillouin formula for the "nuclear" S matrix and the exact quantum mechanical orbiting Regge pole. The oscillatory behavior of the reflection function η_l of the $^{16}O+^{28}Si$ system at $E_{lab}=55$ MeV as a function of l for l below the orbiting region is also explained.

[NUCLEAR REACTIONS ^{16}O-^{28}Si scattering at $E_{lab}=55$ MeV. Analysis of orbiting phenomena. Regge poles related to orbiting.]

I. INTRODUCTION

The experimental results of Braun-Munzinger *et al.*[1] on the scattering of ^{16}O by ^{28}Si at $E_{lab}=55$ MeV is a very interesting case in heavy ion scattering (HIS). The most dramatic feature of their data is the rapid oscillation of the rather large differential cross section in the back angle region. The theoretical analysis of this problem has generated several potentials referred to as the E18, SD, GK, and LC potentials.[2] The E18 potential does not fit the large angle data. Among these potentials, the LC potential is the most impressive and fits the data quite well at all angles.

Because of the close similarity of the large angle oscillations and the behavior of $|P_l(\cos\theta)|^2$ for a suitable $l=l_g$, the natural choice of Braun-Munzinger *et al.* was to fit the data in that region by a Regge pole term. This is essentially a parametrization of the data and does not throw as such much light on the underlying physical phenomena occurring in the generation of large back angle scattering. Mermaz[3] has analyzed $^{16}O+^{28}Si$ data by including fluctuation terms in the parametrized S matrix. The success of the LC potential is very impressive and one is inclined to believe that this potential implicitly incorporates the essential physical process occurring in $^{16}O+^{28}Si$ scattering at $E_{lab}=55$ MeV. In order to establish the role of *exact* Regge poles in the analysis of this problem, Takemasa and Tamura[2] have computed the cross sections generated by the exact Regge poles and the corresponding background term for a number of potentials including the LC potential. One curious finding of their work is the close similarity between the cross sections generated by pole terms on one hand and by the background terms on the other. It is desirable to determine if this is more a coincidence or a manifestation of some interesting physical phenomena, and this forms one of the objectives of the present paper.

The main objective of this paper is to explore the

 ©1983 The American Physical Society

key physical process that is occurring in the $^{16}O+^{28}Si$ scattering under consideration. We find that this phenomenon is the orbiting mechanism occurring predominantly in three partial waves in the vicinity of the barrier. We consider all partial waves other than these three as belonging to the background. We show that the back angle scattering features are the result of a very interesting kind of almost destructive interference between the orbiting partial waves and the background partial waves. With our approach it is possible to explain why the exact Regge background term generates a behavior similar to that of the pole term. We can also understand the correlation between exact Regge poles and the orbiting phenomena and how a *parametric* Regge pole is able to incorporate the effect of both the Regge background amplitude plus the amplitude from the *exact* Regge poles. We further study the poles occurring in the WKB formula for phase shift and exact Regge poles.

The plan of the paper is as follows. In Sec. II we examine the features pertaining to orbiting in quantum scattering and use them to analyze $^{16}O+^{28}Si$ scattering. In Sec. III the interplay between orbiting partial waves and background is examined. This section also contains the analysis of the similarity of pole terms and background terms in a Regge-type analysis and related aspects. In Sec. IV we further examine the orbiting mechanism and other features such as the relation between the poles of the Wentzel-Kramers-Brillouin (WKB) formula for the "nuclear" S matrix and the exact Regge poles associated with orbiting. Section V contains concluding remarks.

II. ORBITING PHENOMENA IN QUANTUM SCATTERING

Let us consider the effective potential

$$V_{\text{eff}}(L,r)=V(r)+\frac{L^2}{2mr^2} \tag{1}$$

which describes the motion of a particle of mass m, energy E, and angular momentum L in classical dynamics. While approaching the potential center, the particle can get trapped in a circular orbit of radius r_0 if $E=V_{\text{eff}}(L,r_0)>0$, and r_0 is the position of maxima of $V_{\text{eff}}(L,r)$. This is because at $r=r_0$, radial kinetic energy $K_r=0$, and $L^2/2mr^2$ accounts for the rotational kinetic energy. If $V_{\text{eff}}(L,r)$ is reasonably flat around $r=r_0$, then the particle having energy slightly different from $V_{\text{eff}}(L,r_0)$ will also spend a considerable length of time in the region $r\sim r_0$ undergoing mostly rotational motion or orbiting. Thus, what characterizes orbiting or almost orbiting phenomena in classical mechanics is the motion with $K_r=0$ or $K_r\simeq 0$ in the neighborhood of the barrier of $V_{\text{eff}}(L,r)$. To carry out the analysis of orbiting phenomena in a completely quantum mechanical HIS formalism, we express the effective potential as

$$V_{\text{eff}}(l,r)=V_n(r)+iW_n(r)+V_c(r)+l(l+1)/r^2 . \tag{2}$$

Here we have adopted $\hbar=2\mu=1$ unit. $(V_n(r)+iW_n(r))$ is the nuclear optical potential $V_N(r)$, $V_c(r)$ is the electrostatic potential, and $l(l+1)/r^2$ is the centrifugal term. Now we observe that in the case of HIS and in the neighborhood of $r=R_B$ corresponding to the maxima of $\text{Re}(V_{\text{eff}}(l,r))$,

$$|\Delta V_{\text{eff}}(l,r)| = |V_{\text{eff}}(l+1,r)-V_{\text{eff}}(l,r)| \ll |V_{\text{eff}}(l,r)| . \tag{3}$$

For example, one finds $\text{Re}V_{\text{eff}}(0,R_B)\simeq 20.3$ fm^{-2} and $R_B\sim 9.74$ fm in the case of the HIS potential[4] describing $^{18}O+^{58}Ni$ scattering at $E_{\text{lab}}=60$ MeV, whereas

$$\Delta V_{\text{eff}}(l,r)\simeq(2l+1)/R_B{}^2 .$$

This is only ~ 0.53 fm^{-2} even for a large, partially absorbed surface region partial wave $l=25$. Hence, if $k^2=\text{Re}\ V_{\text{eff}}(l,R_B)$ for a surface region partial wave $l=l_0$, $k^2\simeq\text{Re}V_{\text{eff}}(l,R_B)$ even for neighboring partial waves like $l=l_0\pm 1$. In addition, if $\text{Re}V_{\text{eff}}(l,r)$ is reasonably flat around $r=R_B$, $l\sim l_0$, then it is reasonable to expect that several partial waves, and in particular those with $l=l_0$, $l_0\pm 1$, will undergo orbiting phenomena around the barrier. This gives rise to the possibility of these partial waves acting in coherence to generate a characteristic feature in the scattering data. From these considerations we find that in order to make a clear analysis of orbiting phenomena in HIS one should examine whether $V_{\text{eff}}(l,r)$ is reasonably flat for a set of a few partial waves which are not fully absorbed and for which $V_{\text{eff}}(l,R_B)\simeq k^2$. If this criterion is satisfied, an appropriate signature in the behavior of the quantal wave function correlated with orbiting should be identified.

For this purpose we consider the (modified) radial Schrödinger equation in $\hbar=2\mu=1$ unit:

$$\frac{d^2}{dr^2}\phi(l,k,r)+\left[k^2-V(r)-\frac{l(l+1)}{r^2}\right]\phi(l,k,r)=0 . \tag{4}$$

The operator

$$\left[-\frac{d^2}{dr^2}\right]$$

is clearly associated with the radial kinetic energy K_r. If

$$|\phi''(l,k,r)| \ll |\phi(l,k,r)|$$

and is close to zero in the region $R_B-\Delta<r<R_B+\Delta$, that implies that the average radial kinetic energy K_r around $r=R_B$ is small and most of the mechanism is owing to orbiting. If this feature manifests only in one partial wave and Δ is too small, it may not be able to generate a measurable effect in HIS data since a large number of other partial waves are also contributing. Therefore it is important to see if it happens to a set of partial waves over a fairly wide range. Then it can be expected to give rise to measurable effects. We demonstrate that this is the phenomenon occurring in the $^{16}O+^{28}Si$ scattering under investigation.

The remarkable success of the LC potential in fitting the $^{16}O+^{28}Si$ data at $E_{lab}=55$ MeV makes it our natural choice for the analysis of orbiting. That our results pertain primarily to the physical process occurring in the $^{16}O+^{28}Si$ system and not a special feature of the LC potential will be made clear at a later stage by reproducing the essential features with the SD potential. Figure 1 shows $\mathrm{Re}V_{\mathrm{eff}}(l,r)$ for several l as a function of r for the $^{16}O+^{28}Si$ system at the $E_{lab}=55$ MeV with the LC potential describing the nuclear interaction. The form of the LC potential is different from the usual Woods-Saxon form and is given by

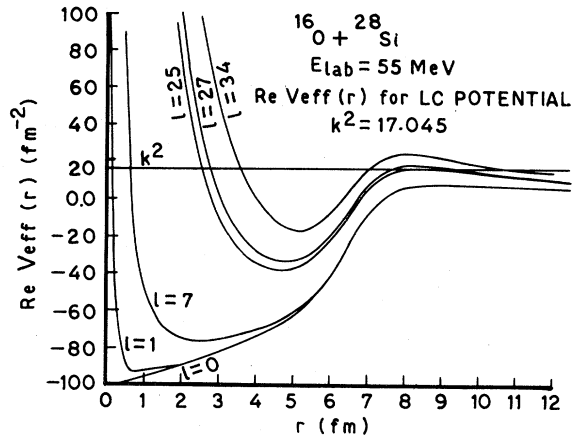

FIG. 1. $\mathrm{Re}V_{\mathrm{eff}}(l,r)$ for a set of l corresponding to the LC potential and the $^{16}O+^{28}Si$ system at $E_{lab}=55$ MeV. $V_{\mathrm{eff}}(l,r)$ for $l=24,26$ are too close to $l=25$ and hence not shown.

$$V(r)=(286.5+19.7i)\left[1.+0.99\exp\left[\frac{r-R}{3.7}\right]+\exp\left[\frac{r-R}{0.49}\right]\right]^{-1}\ \mathrm{MeV}\ ,$$

$$R=1.122(A_1^{1/3}+A_2^{1/3})\ \text{and}\ r_c=1.2\ \text{fm}\ .$$

$V_{\mathrm{eff}}(l,r)$ for $l=24,26$ are too close to that of $l=25$ and hence are not shown in the figure. It is clear that orbiting phenomena are most likely to occur for the set $l=24,25,26$ and around $R_B\sim 8.4$ fm. The effective potential appears reasonably flat in this region, but a further clarification of "reasonable flat" is desirable. We do this by making a comparative study of $V_{\mathrm{eff}}(l,r)$ for $^{18}O+^{58}Ni$ at 60 MeV and that of $^{16}O+^{28}Si$ given in Fig. 1. $V_{\mathrm{eff}}(l,r)$ for the former is computed from the optical potential of Ref. 4. $^{18}O+^{58}Ni$ scattering considered here is a typical case of HIS and does *not* show back angle oscillations, and therefore is suitable for comparison purpose. Figure 2 shows the $V_{\mathrm{eff}}(l,r)$ for both of these cases in the surface region along with

$$\frac{d}{dr}V_{\mathrm{eff}}(l,r)$$

for appropriate partial waves. The latter gives further clarification of the notion of flatness of $V_{\mathrm{eff}}(l,r)$ and shows that the $^{16}O+^{28}Si$ effective potential is significantly flatter around the barrier, further indicating the possibility of the occurrence of quantal orbiting phenomena for $l=24,25,26$. The partial waves $l<24$ are highly absorptive and for $l>26$ barrier reflection can be expected to be the major physical process. In the $^{18}O+^{58}Ni$ case $V_{\mathrm{eff}}(l,r)$ falls rather steeply on either side of the barrier ($R_B\sim 9.5$ fm), making significant and stable orbiting unlikely for a consecutive set of partial waves.

In Figs. 3–5 the variations of $\phi(l,k,r)$ and $\phi''(l,k,r)$ in the barrier region are shown for $l=24,25,26$. $\phi(l,k,r)$ is the regular solution of Eq. (4) behaving like r^{l+1} near the origin and is computed by integrating in steps of $h=0.01$ fm. The constants C_l are such that $\phi(l,k,h_0)=10^{-6}$ with $h_0=(l+1)h$. It is well known that $\phi(l,k,r)$ for a complex potential builds up very rapidly, resulting in large values of C_l. However, it is the relative behavior of $\phi(l,k,r)$ and $\phi''(l,k,r)$ in the surface region which is of crucial significance for our purposes. Figures 3(a), 4(a), and 5(a) indicate the rapid buildup of $\phi(l,k,r)$ in the barrier region around

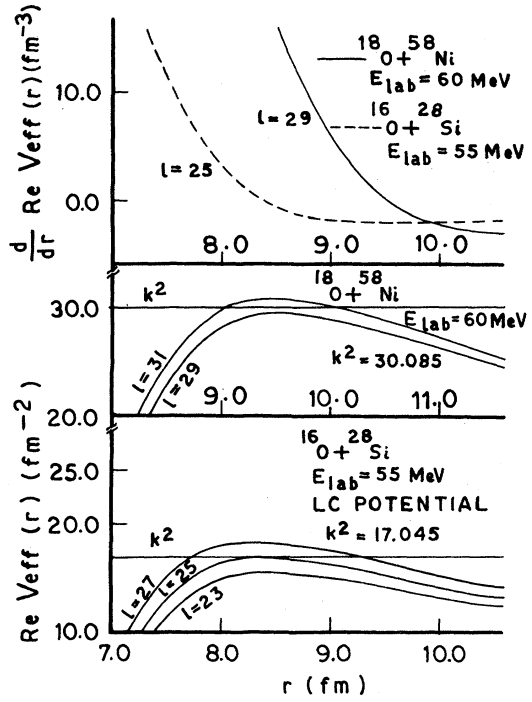

FIG. 2. Behavior of $\mathrm{Re}V_{\mathrm{eff}}(l,r)$ and

$$\frac{d}{dr}V_{\mathrm{eff}}(l,r)$$

for two systems: (i) ^{16}O+^{28}Si at $E_{\mathrm{lab}}=55$ MeV and (ii) ^{18}O+^{58}Ni at $E_{\mathrm{lab}}=60$ MeV. The nuclear potential in case (ii) is of Woods-Saxon form with $V_0=90.1$ MeV, $W_0=42.9$ MeV, $R=R'=7.92$ fm$=R_c$, and $a=0.49$ fm.

$R_B=8.5$ fm. Comparatively speaking $\phi''(l,k,r)$ is very small over a fairly wide region of about 1 fm around R_B [Figs. 3(b), 4(b), and 5(b)]. The result for $l=25$ is the most dramatic, indicating negligible K_r over a considerable range of ~ 0.3 fm, implying the predominance of orbiting. The interesting questions that will be examined now are (i) whether all three orbiting partial waves can contribute coherently to the amplitude and (ii) what the respective roles of orbiting partial waves and the background partial waves are in generating back angle oscillations. We will consider the second question first.

We express the scattering amplitude $A(\theta)$ as a sum of the Coulomb amplitude $A_c(\theta)$ and the "nuclear" amplitude $A_N(\theta)$

$$A(\cos\theta)=A_c(\theta)+A_N(\theta)\ , \tag{5}$$

where

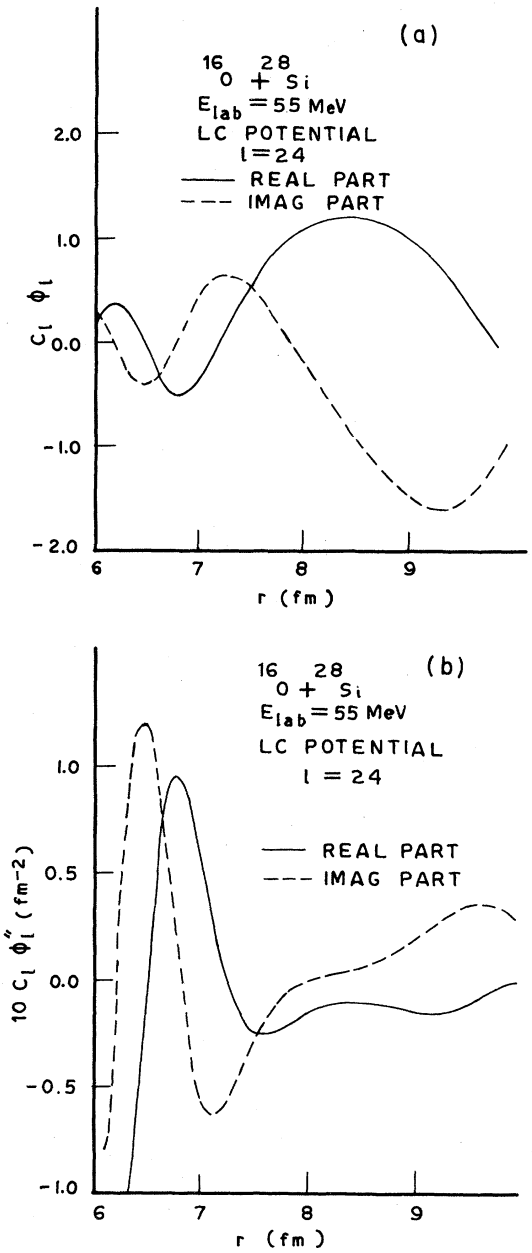

FIG. 3. (a) Behavior of the regular wave function $\phi(l,k,r)$ on the surface region for the LC potential and $l=24$. $C_l=10^{18}$. (b) Behavior of $\phi''(l,k,r)$ on the surface region for the LC potential and $l=24$. $C_l=10^{18}$.

$$A_c(\theta)=\frac{-\eta}{2k\sin^2\frac{\theta}{2}}\exp\left[-i\eta\ln\sin^2\frac{\theta}{2}+2i\sigma_0\right]$$

$$=\frac{1}{2ik}\sum_{l=0}^{\infty}(2l+1)e^{2i\sigma_l}P_l(\cos\theta)\ , \qquad 0<\theta\leq\pi \tag{6}$$

and

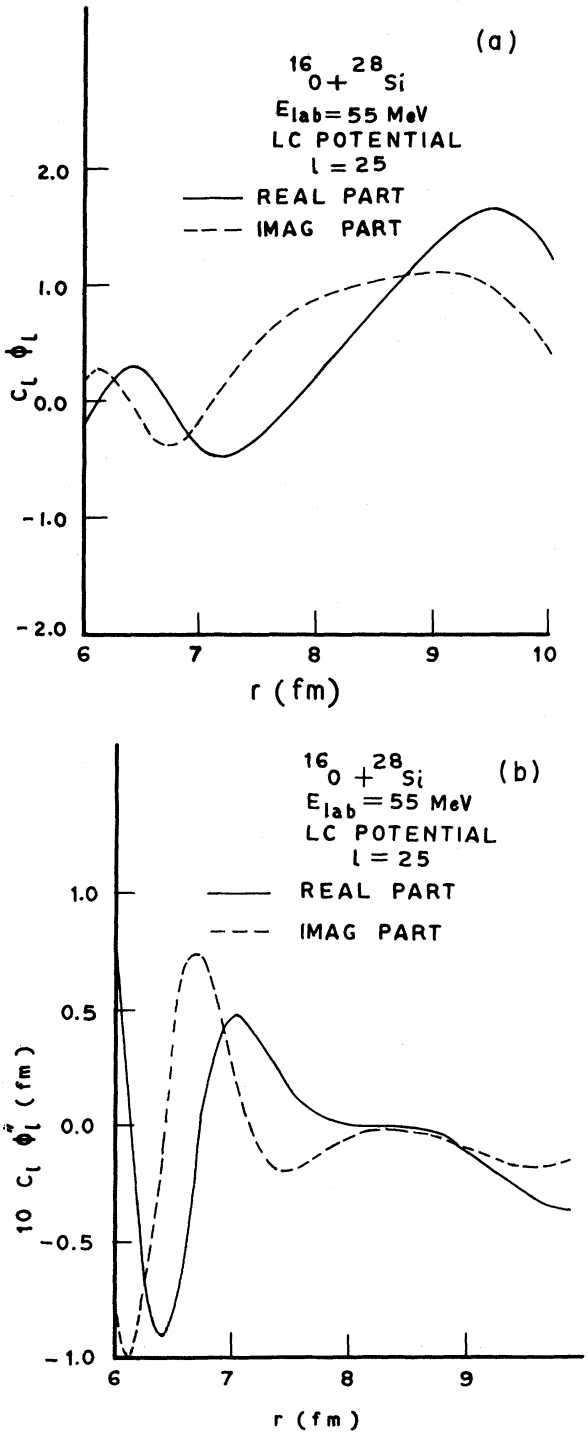

FIG. 4. Same as Fig. 3 for $l=25$. $C_l=10^{19}$.

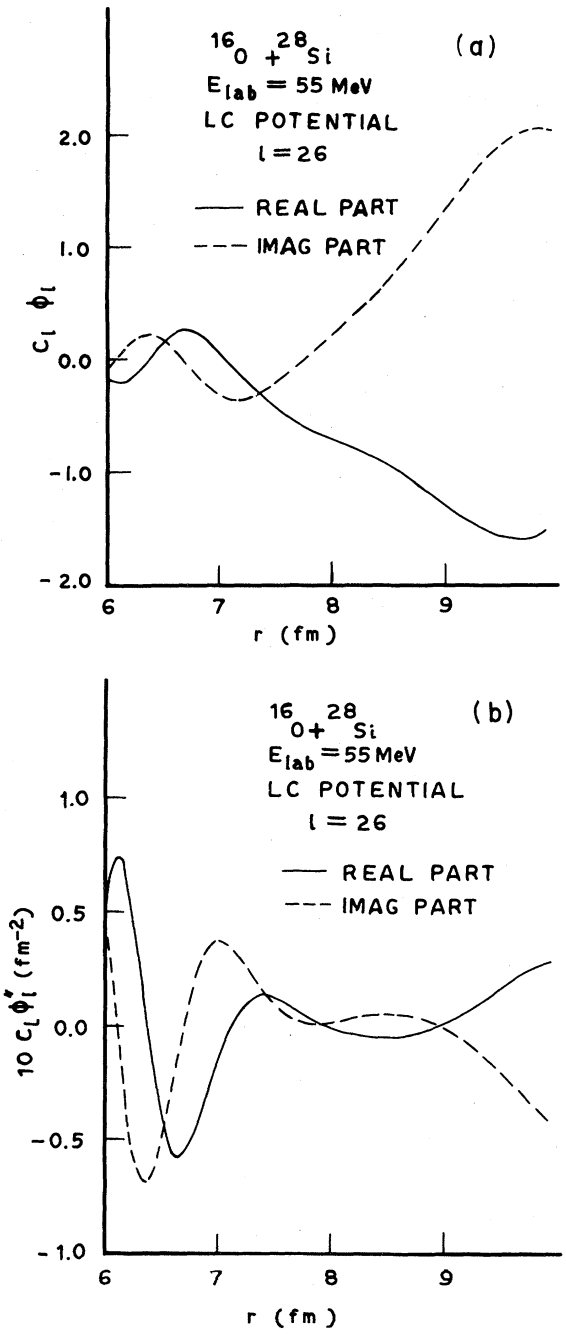

FIG. 5. Same as Fig. 3 for $l=26$. $C_l=10^{20}$.

$$A_N(\theta)=\frac{1}{2ik}\sum_{l=0}^{\infty}(2l+1)e^{2i\sigma_l}\times[S_N(l,k)-1]P_l(\cos\theta)\ . \quad (7)$$

Here η is the Coulomb parameter, σ_l is the Coulomb phase shift, and $S_N(l,k)$ is the nuclear S matrix. Now we define the amplitudes $A_0(\theta)$ and $A_b(\theta)$ associated with the orbiting partial waves and the background partial waves:

$$A_0(\theta)=\frac{1}{2ik}\sum_{l=l_i}^{l=l_f}(2l+1)e^{2i\sigma_l}\times[S_N(l,k)-1]P_l(\cos\theta)\ , \quad (8)$$

$$A_b(\theta)=A(\theta)-A_0(\theta)\ . \tag{9}$$

$l_i \le l \le l_f$ defines the range of orbiting partial waves. In our case $l_i=24$, and $l_f=26$. $\sigma(\theta)$, $\sigma_0(\theta)$, $\sigma_b(\theta)$, and $\sigma_R(\theta)$ are the differential cross sections associated with ampltiudes $A(\theta)$, $A_0(\theta)$, $A_b(\theta)$, and $A_c(\theta)$, respectively. Figures 6(a)–6(c) show $\sigma(\theta)/\sigma_R(\theta)$, $\sigma_b(\theta)/\sigma_R(\theta)$, and $\sigma_0(\theta)/\sigma_R(\theta)$, respectively. All cross sections are computed at 0°,2.5°,5°, . . . , and figures are drawn by making smooth curves over these points. The very close and almost identical

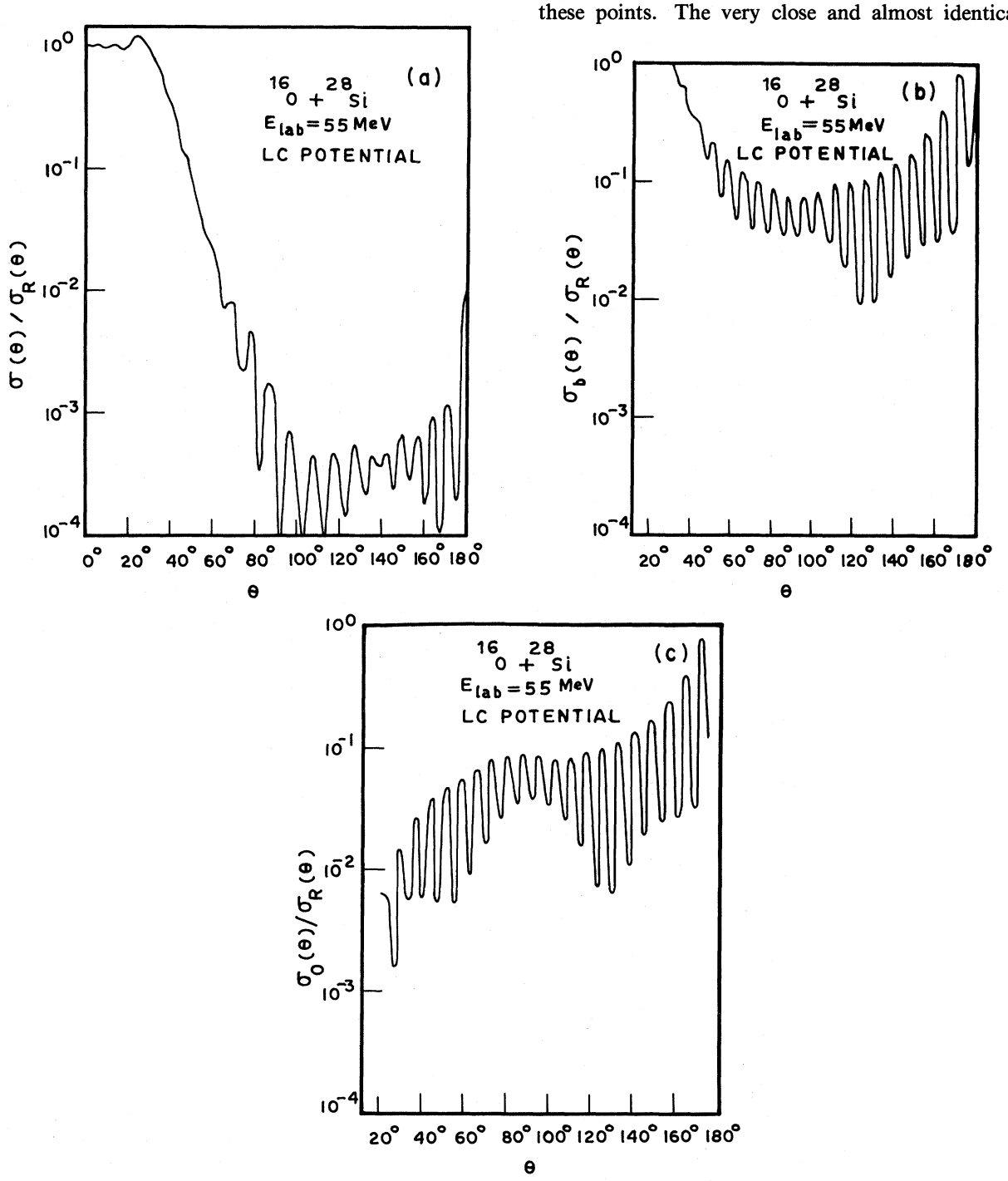

FIG. 6. (a) $\sigma(\theta)/\sigma_R(\theta)$ for $^{16}O+^{28}Si$ at $E_{lab}=55$ MeV generated by the LC potential. (b) $\sigma_b(\theta)/\sigma_R(\theta)$ for $^{16}O+^{28}Si$ at $E_{lab}=55$ MeV generated by the LC potential. (c) $\sigma_0(\theta)/\sigma_R(\theta)$ for $^{16}O+^{28}Si$ at $E_{lab}=55$ MeV generated by the LC potential.

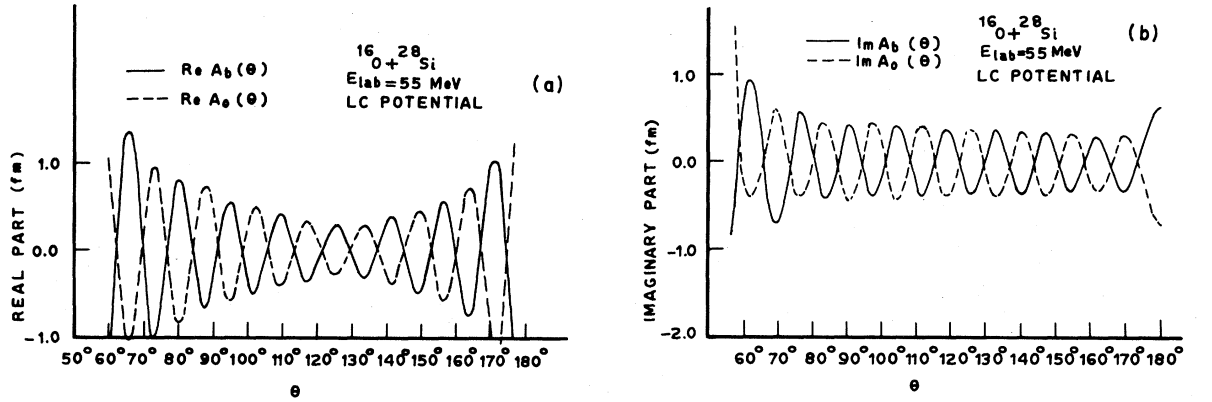

FIG. 7. (a) Variation of $\mathrm{Re}A_0(\theta)$ and $\mathrm{Re}A_b(\theta)$ as a function of θ for the $^{16}O+^{28}Si$ system at $E_{lab}=55$ MeV for the LC potential. (b) Variation of $\mathrm{Im}A_0(\theta)$ and $\mathrm{Im}A_b(\theta)$ as a function of θ for the system specified in Fig. 7(a).

behavior of $\sigma_b(\theta)/\sigma_R(\theta)$ and $\sigma_0(\theta)/\sigma_R(\theta)$ for $\theta \gtrsim 100°$ is striking. Moreover, these are much larger than $\sigma(\theta)/\sigma_R(\theta)$ at large angles.

The obvious explanation of this is the more or less, but not complete, destructive interference between $A_b(\theta)$ and $A_0(\theta)$. In Figs. 7(a) and (b) we show the behavior of these amplitudes as a function of angle, which makes it very clear that orbital amplitude $A_0(\theta)$ is almost out of phase with $A_b(\theta)$. Both $\sigma_0(\theta)/\sigma_R(\theta)$ and $\sigma_b(\theta)/\sigma_R(\theta)$ generate enhanced large angle oscillations. It is the subtle, but not complete, cancellations between $A_b(\theta)$ and $A_0(\theta)$ which are responsible for comparatively reduced, but still significant and enhanced, back angle oscillations; it appears that the orbital amplitude becomes almost out of phase with $A_b(\theta)$ in the process of orbiting. A heuristic mathematical and physical analysis of the origin of this phase difference will be described later.

Before concluding this section we show that the interesting features described above are not a special characteristic of the LC potential; any potential which can fit the $^{16}O+^{28}Si$ data manifests essentially the same features. For this purpose we consider the SD potential[2] which has a Woods-Saxon radial form for both real and imaginary parts, and in the standard notation the potential parameters are the following: $V_0=27.456$ MeV, $r_0=1.31$ fm, $a_0=0.485$ fm, $W_0=4.865$ MeV, $r_I=1.277$ fm, $a_I=0.323$ fm, and $r_c=1.0$ fm. In Fig. 8 we show the behavior of $\phi''(l,k,r)$ for typical $l=26$, which is also on the barrier region and builds up rapidly afterwards. Similarly Figs. 9(a)–(c) show the variation of $\sigma(\theta)/\sigma_R(\theta)$, $\sigma_b(\theta)/\sigma_R(\theta)$, and $\sigma_0(\theta)/\sigma_R(\theta)$, respectively, and generated by the SD potential. The patterns of the back angle oscillations of $\sigma_b(\theta)/\sigma_R(\theta)$ and $\sigma_0(\theta)/\sigma_R(\theta)$ are very similar. It is true that in this case the results are slightly less impressive as compared to those obtained using the LC potential. This should not be surprising because the SD potential does *not* provide as good a fit to $^{16}O+^{28}Si$ data as the LC potential does. However, both potentials retain the feature that both $A_0(\theta)$ and $A_b(\theta)$ generate rapid and large back angle oscillations and they are more or less out of phase generating reduced large angle oscillations in $\sigma(\theta)/\sigma_R(\theta)$. This indicates that subtle, and almost destructive, interference between $A_0(\theta)$ and $A_b(\theta)$ represents a characteristic feature of the $^{16}O+^{28}Si$ collision at $E_L=55$ MeV.

Just for thoroughness and for the purposes of comparison, in Fig. 10 we give $\phi''(l,k,r)$ generated

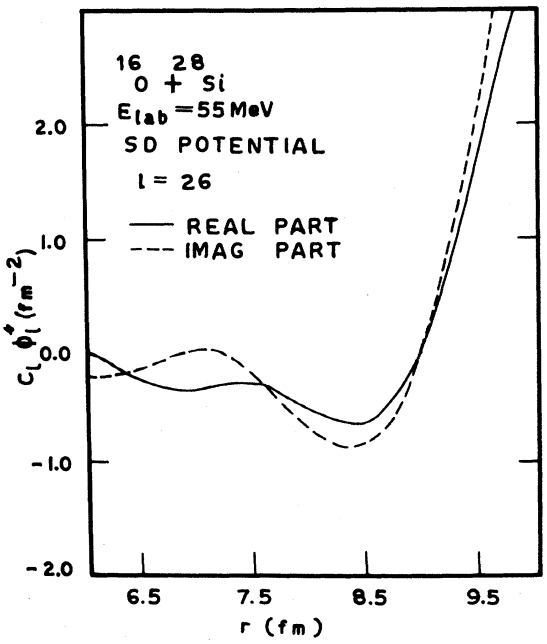

FIG. 8. Variation of $\phi''(l,k,r)$ on the surface region for $l=26$ using the SD potential.

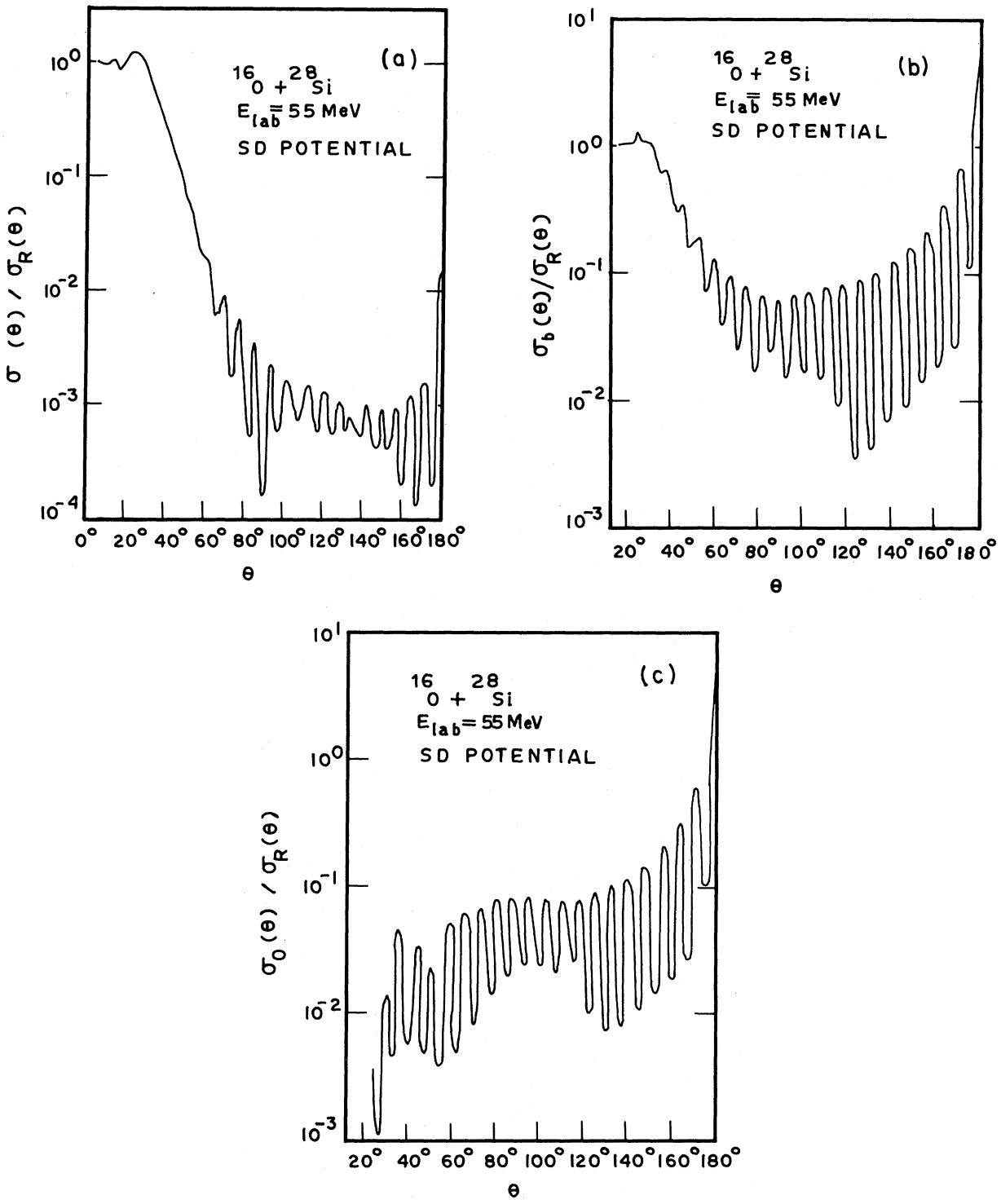

FIG. 9. Same as Fig. 6 with the SD potential.

for $^{16}O+^{28}Si$ for the $l=24,25,26$ system at 55 MeV for the LC potential *without* the imaginary part. In this case, one also finds the reduced values of $\phi''(l,k,r)$ around the barrier region. It is, however, worth noting that the physical characteristics generated by a real potential will be different from the HIS case because of the absence of more or less complete absorption of lower partial waves. We will not discuss further the case of real potential orbiting.

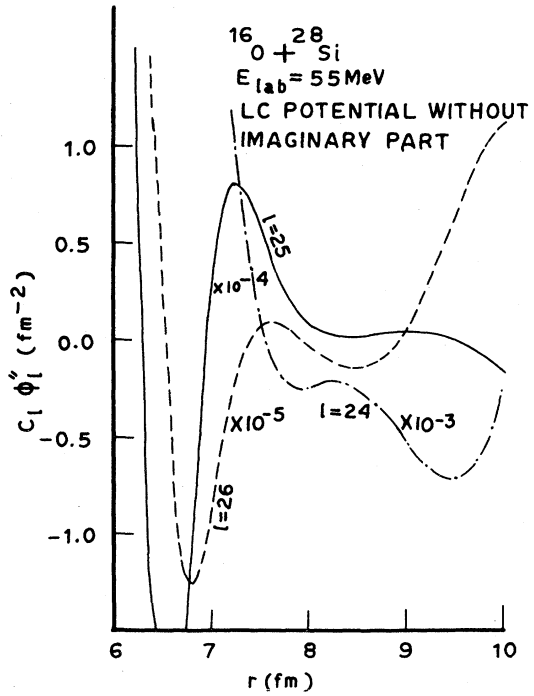

FIG. 10. Variation of $\phi''(l,k,r)$ for $l=24,25,26$ for the $^{16}O+^{28}Si$ system at $E_{lab}=55$ MeV obtained by setting $W_n(r)=0$, in the LC potential.

III. ORBITAL WAVE AND BACKGROUND WAVE INTERFERENCE

In order to further elucidate the nature and origin of the interference between $A_0(\theta)$ and $A_b(\theta)$ we write

$$A_b(\theta)=A_{\text{int}}(\theta)+A_{\text{ext}}(\theta)\ , \tag{10}$$

where

$$A_{\text{int}}(\theta)=\sum_{l=0}^{l_i-1}(2l+1)e^{2i\sigma_l}S_N(l,k)P_l(\cos\theta) \tag{11}$$

and $A_{\text{ext}}(\theta)$ then gets defined by (10). Highly absorbed partial waves, for most of which $|S_N(l,k)|\simeq 0$, contribute to $A_{\text{int}}(\theta)$, and therefore we expect $A_{\text{ext}}(\theta)$ to give a dominant contribution to $A_b(\theta)$ and hence to the interference betweeen $A_0(\theta)$ and $A_b(\theta)$. This is demonstrated by Figs. 11 and 12. In Fig. 11 we show the variation of $A_0(\theta)$ and $A_{\text{ext}}(\theta)$ in the large angle region $120°\leq\theta\leq 180°$. Figure 12 shows the variation of $A_{\text{int}}(\theta)$ in the same region. Comparison of Figs. 7 and 11 makes it clear that the $A_{\text{ext}}(\theta)$ plays the major role in the dramatic interference between $A_0(\theta)$ and $A_b(\theta)$. That is, the primary physical phenomenon which occurs at large angles is the interference between the orbiting partial waves and the external, Coulomb dominated partial waves.

Now, since $A_0(\theta)$ has only three orbiting partial waves, it is reasonable to expect that they can be reproduced by the Regge-type representations[5] of the nuclear partial wave amplitudes in terms of the exact poles in the orbiting region of l. This will be discussed in Sec. IV. The dominant poles will take into account a substantial part of the $A_0(\theta)$. Similarly $A_b(\theta)$, and to a little lesser extent $A_{\text{ext}}(\theta)$, should account for most of the Regge background. Now we will demonstrate mathematically that the large angle variation of both $A_0(\theta)$ and $A_{\text{ext}}(\theta)$ is dominated by the *same* Legendre polynomial. In a somewhat more approximate sense, $A_{\text{int}}(\theta)$ is also dominated by the same Legendre polynomial at large angles. Identifying $A_0(\theta)$ with the pole dominated part of the amplitude, and $A_b(\theta)$ or $A_{\text{ext}}(\theta)$ with the Regge background dominated part of the amplitude, we immediately obtain a heuristic *mathematical* explanation for the similarity in the cross sections generated by pole terms and Regge background terms observed in Ref. 2.

In order to do this we first examine the variation of the reflection function

$$\eta_l=|S_N(l,k)|$$

as a function of l in the caes of (i) $^{16}O+^{28}Si$ at $E_{lab}=55$ MeV and (ii) $^{18}O+^{58}Ni$ at $E_{lab}=60$ MeV (Fig. 13). The latter does not show back angle enhanced oscillations. In Table I we also list S-matrix elements for $23\leq l\leq 29$. The transition from almost complete absorption ($\eta_l\simeq 0$) to almost pure Coulomb scattering ($\eta_l\simeq 1$) is more rapid in the $^{16}O+^{28}Si$ case and the most important partially absorbed ($0<\eta_l<1$) partial waves are the orbiting waves. In the $^{18}O+^{58}Ni$ case this transition is rather slow. We notice that in the absorption region of

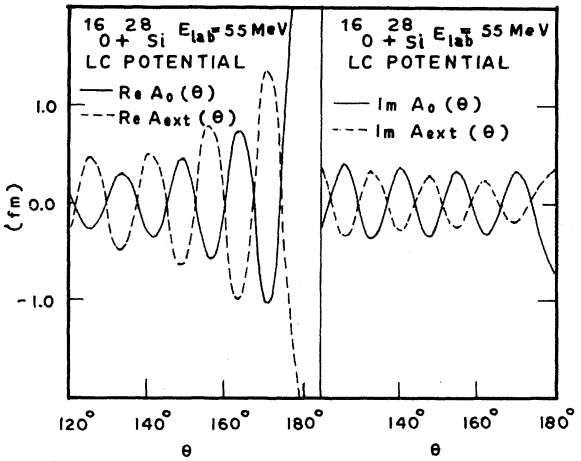

FIG. 11. Variation of $A_0(\theta)$ and $A_{\text{ext}}(\theta)$ with θ for the system specified in Fig. 7(a).

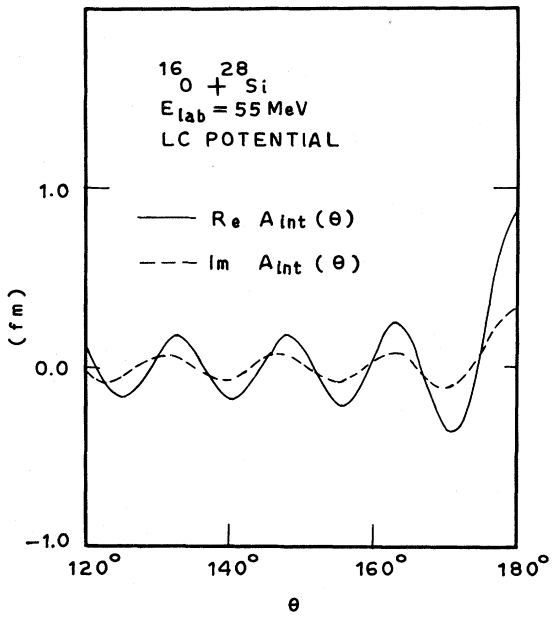

FIG. 12. Variation of $A_{\text{int}}(\theta)$ with θ for the system specified in Fig. 7(a).

^{16}O+^{28}Si, even though $\eta_l \simeq 0$, it shows l-dependent structure which is absent in the ^{18}O+^{58}Ni case. The reason for this will be examined later. In view of the former observation and also for the purpose of demonstrating the results *analytically,* we approximate $S_N(\lambda,k)\simeq 1$ for $l > l_f$ in the case of ^{16}O+^{28}Si and write

$$A_{\text{ext}}(\theta)\simeq \tilde{A}_{\text{ext}}(\theta) = \frac{1}{2ik}\sum_{l_i=L}^{\infty}(2l+1)e^{2i\sigma_l}P_l(\cos\theta)\ . \tag{12}$$

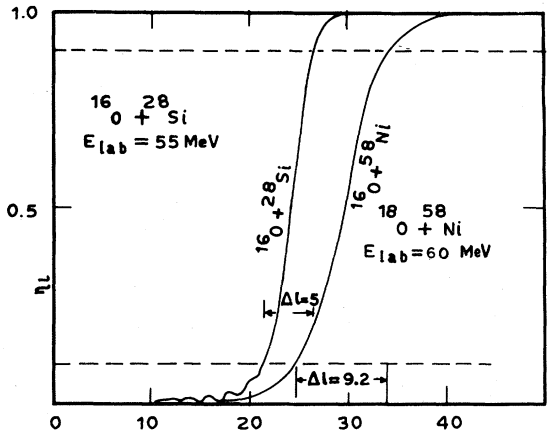

FIG. 13. Variation of the reflection function η_l as a function of l for (i) ^{16}O+^{28}Si at $E_{\text{lab}}=55$ MeV and (ii) ^{18}O+^{58}Ni at $E_{\text{lab}}=60$ MeV. Potential for the latter is specified under Fig. 2. Δl is the change in l when η_l grows from $\eta_l=0.1$ to $\eta_l=0.9$.

Now we note that l_i is large. In our particular case $l_i=L=24$. In order to determine the dominant behavior of $A_{\text{ext}}(\theta)$ we proceed as follows.

$$\sigma_l=\arg\Gamma(l+1+i\eta)\ . \tag{13}$$

But[6]

$$\arg\Gamma(x+iy)=y\frac{\Gamma'(x)}{\Gamma(x)} + \sum_0^{\infty}\left[\frac{y}{x+n}-\arctan\left[\frac{y}{x+n}\right]\right]. \tag{14}$$

We can further simplify this to obtain

$$\arg\Gamma(x+iy)=y\frac{\Gamma'(x)}{\Gamma(x)} + \sum_0^{\infty}\left[\frac{1}{3}\left[\frac{y}{x+n}\right]^3-\frac{1}{5}\left[\frac{y}{x+n}\right]^5 + \cdots\right]. \tag{15}$$

Similarly,

$$\frac{\Gamma'(x)}{\Gamma(x)}=\ln x-\frac{1}{2x}+0(x^{-2})\ .$$

Since x is large ($x\geq L+1=25$ in our case), and y ($=\eta=9.51$) is much smaller compared to x, we obtain to the leading order and for large $l\geq L$,

$$\sigma_l\simeq\eta\ln(l+1)\ . \tag{16}$$

Therefore we approximate

$$\tilde{A}_{\text{ext}}(\theta)=\frac{1}{2ik}\sum_L^{\infty}(2l+1)(l+1)^{2i\eta}P_l(\cos\theta)\ . \tag{17}$$

Now we evaluate (17) using the Poisson summation method.[7] We write

$$\tilde{A}_{\text{ext}}(\theta)=\frac{1}{2ik}\sum_{m=-\infty}^{\infty}\int_L^{\infty}(2l+1)(l+1)^{2i\eta} \times e^{2iml\pi}P_l(\cos\theta)dl\ . \tag{18}$$

For large angles $m=0$ is the most dominant term.[6] Also we approximate

$$(2l+1)(l+1)^{2i\eta}\simeq 2\lambda^{2i\eta+1}\ ,$$
$$\lambda=l+\tfrac{1}{2}\ .$$

Then one gets

$$\tilde{A}_{\text{ext}}(\theta)\simeq\frac{1}{ik}\int_{\Lambda}^{\infty}d\lambda\,\lambda^{2i\eta+1}P_{\lambda-1/2}(\cos\theta)\,,$$

$$\Lambda=L+\tfrac{1}{2}\,. \quad (19)$$

But for large λ we have

$$P_{\lambda-1/2}(\cos\theta)=[(\pi/2)\lambda\sin\theta]^{-1/2}\times\cos[\lambda\theta-\pi/4]\,. \quad (20)$$

Substituting (20) in (19) and integrating we get

$$\tilde{A}_{\text{ext}}(\theta)\simeq\frac{1}{ik}(\pi\sin\theta)^{-1/2}\theta^{-2i\eta-3/2}\times[\,C(\Lambda\theta,2i\eta+\tfrac{3}{2})+S(\Lambda\theta,2i\eta+\tfrac{3}{2})]\,, \quad (21)$$

where C and S are Fresnel integrals[8]

$$C(x,\alpha)=\int_{x}^{\infty}t^{\alpha-1}\cos t\,dt\,, \quad (22)$$

$$S(x,\alpha)=\int_{x}^{\infty}t^{\alpha-1}\sin t\,dt\,. \quad (23)$$

Using the leading terms in the asymptotic expansions for $C(x,\alpha)$ and $S(x,\alpha)$ (Ref. 8, p. 150) one obtains

$$\tilde{A}_{\text{ext}}(\theta)\simeq\frac{2^{1/2}}{ik}\frac{(\pi\sin\theta)^{-1/2}}{\theta}\Lambda^{2i\eta-1/2}\times\left[\Lambda\cos(\Lambda\theta+\pi/4)+\frac{\cos(\Lambda\theta-\pi/4)}{\theta}\right]$$
$$\simeq\frac{\Lambda^{2i\eta}}{ik\theta}\left[\Lambda P_{\Lambda-1/2}(\cos\theta')-\frac{1}{\theta}P_{\Lambda-1/2}(\cos\theta)\right],\quad\theta\lesssim\pi\,, \quad (24)$$

where $\theta'=\theta+\pi/2\Lambda\simeq\theta$, and for large Λ, $\theta\lesssim\pi$.

Therefore, the leading term analysis shows

$$\bar{A}_{\text{ext}}(\theta)\approx\frac{1}{2ik}\left\{\frac{2\Lambda^{2i\eta}}{\theta}(\Lambda-1/\theta)\right\}P_L(\cos\theta)\,,\quad\theta\lesssim\pi\,. \quad (25)$$

Equation (25) clearly shows that for large angle $\bar{A}_{\text{ext}}(\theta)$ is dominated by a single Legendre polynomial which explains the mathematical origin of the similarity of behavior of the Regge background term and the Regge pole amplitudes.

Now let us consider the $A_0(\theta)$ for the $^{16}O+^{28}Si$ case:

$$A_0(\theta)=\frac{1}{2ik}\sum_{l_i}^{l_f}(2l+1)e^{2i\sigma_l}[S_N(l,k)-1]\times P_l(\cos\theta)\,. \quad (26)$$

We recall that $l_i=L=24$, $l_f=26$, and set

$$\bar{L}=(l_i+l_f)/2=L+1\,.$$

Using (20) it is easy to see that for large angles $160^\circ\lesssim\theta\leq180^\circ$ we can have the following approximations with errors of $\sim10\%$:

$$P_{\bar{L}}(\cos\theta)=-P_{l_i}(\cos\theta)=-P_{l_f}(\cos\theta)\,.$$

Therefore, for large angles $\theta\lesssim\pi$,

$$A_0(\theta)\simeq\frac{1}{2ik}\left\{\sum_{l_i}^{l_f}(2l+1)e^{2i\sigma_l}[S_N(l,k)-1](-1)^{\bar{L}-l}\right\}P_{\bar{L}}(\cos\theta)\,. \quad (27)$$

In order to stress our point we computed the quantities in the curly brackets in (25) and (27) at $\theta=\pi$. They have magnitudes of approximately 16.03 and 34.88, respectively. More important, their respective phases, -70° and -75°, are approximately the same; that is, they are approximately in phase. From (20) it is clear that in the neighborhood of $\theta=180^\circ$, $P_L(\cos\theta)$ and $P_{\bar{L}}(\cos\theta)$ will be almost out of phase because $\bar{L}=L+1$, and $\theta\lesssim\pi$. This clearly demonstrates that one can expect $A_0(\theta)$ and $\bar{A}_{\text{ext}}(\theta)$ to be approximately out of phase for large angles. It is as though the partial waves which are undergoing orbiting gain an extra phase due to orbiting. A possible physical explanation for this will be given in Sec. V.

Equation (27) further demonstrates why a *phenomenological* single pole Regge representation should be able to account for the $A_0(\theta)$ and the similarity of the behavior of the pole term amplitude and background amplitude in a Regge analysis in the $^{16}O+^{28}Si$ scattering. Furthermore, we note that if one approximates for $\theta\lesssim\pi$

$$A(\theta)\simeq A_0(\theta)+\bar{A}_{\text{ext}}(\theta)\,. \quad (28)$$

Using (25) and (27) one can write

$$A(\theta)\simeq\frac{1}{2ik}\left\{\frac{2\Lambda^{2i\eta}}{\theta}(\Lambda-1/\theta)-\sum_{l_i}^{l_f}(2l+1)e^{2i\sigma_l}[S_N(l,k)-1](-1)^{\bar{L}}\right\}P_L(\cos\theta)\ . \tag{29}$$

For θ close to π the quantity in the curly bracket in (29) is almost independent of θ, and hence $A(\theta)$ given by (29) is dominated by a single *Legendre polynomial* at large angles. This analysis neatly elucidates the origin of large angle oscillations in ^{16}O+^{28}Si scattering and *explains* the mathematical and physical reason for the success of a *phenomenological* Regge pole representation (without background) in the analysis of large angle data. The orbiting phenomena taking place in a few partial waves are in a sort of coherence and their almost destructive interference with the amplitude generated by peripheral partial waves results in the dominance of a single Legendre polynomial in the large angle region. This conclusion is not affected even if one incorporates $A_{\rm int}(\theta)$, as seen from the numerical results of Sec. II. Moreover, it is possible to examine in an approximate way how $A_{\rm int}(\theta)$ is likely to behave for large angles. In order to do this we write

$$A_{\rm int}(\theta)\simeq\frac{\bar{\epsilon}}{2ik}\sum_{0}^{L-1}(2l+1)P_l(\cos\theta)\ , \tag{30}$$

where $\bar{\epsilon}$ is the average value of $S(\lambda,k)$ (≈ 0) in the absorption region $0\lesssim l\lesssim L-1$.

Using the integral representation[9]

$$P_l(\cos\theta)=\frac{1}{\pi}\int_0^{\pi}(\cos\theta+i\sin\theta\cos t)^l dt\ , \tag{31}$$

we can write

$$A_{\rm int}(\theta)\simeq\frac{\bar{\epsilon}}{2ik\pi}\int_0^{\pi}dt\sum_{0}^{L-1}(2l+1)x^l\ , \tag{32}$$

where

$$x=(\cos\theta+i\sin\theta\cos t)$$
$$\simeq -1+i(\pi-\theta)\cos t+\cdots \tag{33}$$

for $\theta\lesssim\pi$. It is straightforward to carry out the sum in (32). One readily gets

$$\sum_{0}^{L-1}(2l+1)x^l=\frac{1+x}{(1-x)^2}-\frac{2x^{L+1}}{(1-x)^2}-\frac{2L+1}{1-x}x^L\ . \tag{34}$$

Since $x\simeq -1$ for $\theta\lesssim\pi$, and L is large, we get

$$\sum_{0}^{L-1}(2l+1)x^l\simeq-\frac{(2L+1)}{2}x^L-\tfrac{1}{2}x^{L+1}\ . \tag{35}$$

Using this we get for $\theta\lesssim\pi$

$$A_{\rm int}(\theta)\simeq\frac{-\bar{\epsilon}}{4ik\pi}\int_0^{\pi}[(2L+1)x^L+x^{L+1}]dt$$
$$=\frac{-\bar{\epsilon}}{4ik}[(2L+1)P_L(\cos\theta)+P_{L+1}(\cos\theta)],\quad \theta\lesssim\pi \tag{36}$$
$$=\frac{-\bar{\epsilon}L}{2ik}P_L(\cos\theta),\quad \theta\lesssim\pi\ .$$

This heuristic estimate of the large angle behavior of $A_{\rm int}(\theta)$ and the fact that $|S_N(\lambda,k)|\simeq 0$ for $l<l_i$ shows that $A_b(\theta)$ will be dominated by the behavior of the Legendre polynomial $P_L(\cos\theta)$ for $\theta\lesssim\pi$.

Our above analysis leads to the following deductions applicable to the ^{16}O+^{28}Si system at $E_{\rm lab}=55$ MeV:

(a) Orbiting phenomena is predominantly taking place for three important large consecutive partial waves $l=24,25$, and 26, and the asymptotic analysis of the Legendre polynomials indicates that $A_0(\theta)$ behavior is dominated by $P_{\bar{L}}(\cos\theta)$, $\bar{L}=25$. This also indicates that $A_0(\theta)$ can be reasonably well reproduced by quantum mechanical Regge poles in the neighborhood of $\bar{L}$.

(b) Mathematical analysis of $A_{\rm ext}(\theta)$ and $A_{\rm int}(\theta)$ and hence $A_b(\theta)$ indicates that the behavior of $A_b(\theta)$ will be dominated by $P_L(\cos\theta)$ for $\theta\lesssim\pi$ and hence it can be expected to be almost out of phase with $A_0(\theta)$. $A_b(\theta)$ essentially represents the background in an exact Regge pole analysis. This explains the similarity in cross sections[2] generated by exact pole terms and background terms.

(c) Since at $\theta\lesssim\pi$, $A_0(\theta)$ is dominated by $P_{\bar{L}}(\cos\theta)$ and $A_b(\theta)$ by $P_L(\cos\theta)$ with $\bar{L}=L+1$, one essentially gets a single Legendre polynomial dominance [$P_L(\cos\theta)$ *or* $P_{\bar{L}}(\cos\theta)$] in the back angle region. This provides an explanation of the back angle oscillation and the success of *parametric* Regge representation in that region.

Thus we have traced the origin of the large angle entrance oscillations to the presence of orbiting occurring in a few (three) large l partial waves, single Legendre polynomial dominance in both $A_0(\theta)$ and $A_b(\theta)$, and the almost destructive interference between $A_0(\theta)$ and $A_b(\theta)$. Since in other typical HIS the number of important partial waves for which $S_N(l,k)$ is neither close to zero nor unity is

considerably large (Fig. 13), the present analysis will not be applicable. In these cases the dominance of a single Legendre polynomial is unlikely, thereby causing cancellation between different partial waves in the back angle region resulting in high damping of cross sections.

IV. OTHER RELATED FEATURES

In this section we describe several other aspects of $^{16}O+^{28}Si$ scattering related to orbiting.

A. Nuclear molecular resonance

The ^{44}Ti composite system obtained by $^{16}O+^{28}Si$ elastic scattering shows interesting resonance features.[10,11] Of particular interest to us are the resonances at $J=24$ observed at $E_{lab}=55$ MeV, i.e., $E_{c.m.}=35$ MeV. The interpretation of this resonance as being due to orbiting clusters[11] is consistent with our analysis. $V_{eff}(24,r)$ is maximum at $r=8.4$ fm, is flat in the neighborhood, and takes into account almost the entire $E_{c.m.}$. From Figs. 1 and 2, and the fact that the radial wave function builds up very rapidly in this region (Figs. 3–5, we can conclude that the resonance at $E_{c.m.}=35$ MeV is an orbiting resonance localized around the barrier and not in the interior well. However, our calculations using the LC potential indicate that the $l=25$ partial wave is an equally good candidate for this resonance, and for $l=26$ the maximum of $V_{eff}(l,r)$ is about 1.2 MeV larger than $E_{c.m.}$. We believe that since $|P_l(\cos\theta)|$, $\theta \lesssim 180°$, with $l=24,25$ will oscillate similarly, the resonance structure at $E_{c.m.}=35$ MeV may be due to an orbiting resonance at both $l=24$ and 25 and perhaps at $l=26$ also.

B. Exact quantum mechanical Regge poles and orbiting

Takemasa and Tamura[2] have listed a number of exact Regge poles for LC and other potentials. The most interesting among these for our discussion is the pole at $\alpha_2=25.14+1.33i$ in the l plane corresponding to the LC potential. Two other poles of interest in the immediate vicinity are $\alpha_1=26.81+1.34i$ and $\alpha_3=23.5+1.72i$. Similarly the leading pole in the SD potential is $\alpha_0=24.80+1.17i$. From these and from the fact that SD and GK potentials fit large angle data quite well, we find that the Regge poles α_2 of the LC potential or α_0 of the SD potential can be associated with the $l=25$ resonance associated with orbiting. The considerably large $\mathrm{Im}\alpha_1$ also indicates that the pole is unlikely to be associated with a sharp resonance generated inside the potential well.

The Regge formalism gives a wide choice for the construction of different types of Regge representations.[5] In Table I we list the $(S_N(l,k)-1)$ generated by the representation

$$S_N(l,k)-1=\sum \beta_n e^{\frac{-(\lambda-\lambda_n)^2\xi^2}{\lambda-\lambda_n}}, \tag{37}$$

$$\lambda=l+\tfrac{1}{2},\ \lambda_n=\alpha_n+\tfrac{1}{2},\ \xi=0.21,$$

using the poles α_2 and α_3 and residues β_2 and β_3 of $S_N(l,k)$ for the LC potential.[2] The results show that the important orbiting partial wave amplitudes are fairly well reproduced by the Regge representation using the poles in the barrier region. However, in view of the extremely subtle cancellations involved between $A_0(\theta)$ and $A_b(\theta)$ in generating the observed back angle data, for *quantitative* calculations $A_0(\theta)$ generated by the exact pole parameters in the orbiting region without the inclusion of the corresponding background terms will not be adequate. Evaluation of exact quantum mechanical Regge poles is of interest for a better understanding of the physical phenomena associated with resonance structures. However, for the purpose of fitting the data at the back angle region, perhaps a purely parametric Regge pole is suitable since it can be made to take into account both $A_0(\theta)$ and $A_b(\theta)$ as explained in Sec. III. Naturally the real part of such a parametric Regge pole will be close to the orbiting partial wave.

C. Quantal and semiclassical Regge poles

The application of the WKB method for the analysis of HIS is rather extensive. We will in particular consider here the approach of Brink and Takigawa.[12] We assume that there are only three important WKB turning points r_1, r_2, and r_3 in the vicinity of real axis in the complex r plane. This assumption is valid for the LC potential. Furthermore, we assume $\mathrm{Re}r_1>\mathrm{Re}r_2>\mathrm{Re}r_3$. The range $(\mathrm{Re}r_2,\mathrm{Re}r_1)$ corresponds to the barrier domain. The three turning point WKB expression for $S_N(l,k)$ is[12]

$$S_N(l,k)=\frac{\exp(2i\delta_1)}{N(i\epsilon)}+\frac{\exp(2i\delta_3)}{N(i\epsilon)[N(i\epsilon)+\exp(2iS_{32})]}, \tag{38}$$

where

$$\delta_1=\lim R\to\infty\left\{\int_{r_1}^{R}[k^2-V_N(r)-V_c(r)-\lambda^2/r^2]^{1/2}dr-\int_{r_c}^{R}[k^2-V_c(r)-\lambda^2/r^2]^{1/2}dr\right\}, \tag{39}$$

$$\delta_3=\delta_1+i\pi\epsilon+S_{32}\ , \tag{40}$$

$$S_{ij}=\int_{r_i}^{r_j}[k^2-V_N(r)-V_c(r)-\lambda^2/r^2]^{1/2}dr\ , \tag{41}$$

$$\epsilon=\frac{i}{\pi}S_{12}\ , \tag{42}$$

$$N(i\epsilon)=\frac{(2\pi)^{1/2}}{\Gamma(\frac{1}{2}+i\epsilon)}\exp\left[i\epsilon\ln\left[\frac{i\epsilon}{e}\right]\right]. \tag{43}$$

Here r_c is the Coulomb turning point. If $V_c(r)=2\eta k/r$

$$r_c=[\eta+(\lambda^2+\eta^2)^{1/2}]/k\ . \tag{44}$$

It is clear from (38) that information regarding the barrier region is contained in $N(i\epsilon)$ and therefore can be associated with the orbiting region. Brink[13] relates the poles of $S_N(l,k)$ in the l plane generated by $N(i\epsilon)=0$ with the orbiting phenomenon. Due to the presence of $\Gamma(\frac{1}{2}+i\epsilon)$ in (43) one expects $N(i\epsilon)$ to generate an infinite number of poles in the l plane even though only those close to the real axis in the l plane can be expected to be important. Our examination of exact Regge poles for the LC potential shows that the pole α_2 specified earlier can be interpreted as the dominant, exact, *quantal* Regge pole associated with orbiting. Therefore it is of interest to see the correlation between the exact, quantal orbiting Regge pole and the sequence of poles generated by $N(i\epsilon)$ in the WKB expression (38).

We computed the Regge poles $\lambda_n^{\rm WKB}$ in the λ plane generated by setting $N(i\epsilon)=0$ in the case of the LC potential at $E_{\rm c.m.}=35$ MeV corresponding to $E_{\rm lab}=55$ MeV for the ^{16}O+^{28}Si system. These are given by

$$\lambda_n^{\rm WKB}=25.52+0.187i+(0.041n)i\ ,\quad n=0,1,2,\ldots. \tag{45}$$

The corresponding exact quantal Regge pole[2] is

$$\lambda_2^{QM}=\alpha_2+0.5=25.64+1.33i\ . \tag{46}$$

This shows that the exact quantal orbiting pole is correlated with a sequence of infinitely many poles of the corresponding WKB expression for $S_N(l,k)$ such that $\mathrm{Re}\lambda_n^{\rm WKB}\simeq\mathrm{Re}\lambda_2^{QM}$. However, the nuclear potential in our case is smooth and short range and therefore exact $S_N(l,k)$ cannot have an infinite number of poles in the right half plane. But the WKB expression for $S_N(l,k)$ has a different analytical structure than that in the exact $S_N(l,k)$. This should not be surprising because the WKB method does not conserve all the analytical properties of the S matrix. However, in view of the correlations shown above, Brink's idea[13] of correlating the l-plane zeros of $N(i\epsilon)$ with orbiting is correct within the WKB formalism and the real part of these poles is close to the orbiting l.

TABLE I. Comparison of exact $S_N(l,k)-1$ and those generated by Regge representation (37). The LC potential is used. Pole parameters are from Ref. 2.

l	$S_N(l,k)-1$	
	Exact	Regge representation
23	$-0.817+0.145i$	$-0.646-0.021i$
24	$-0.693+0.291i$	$-0.673+0.216i$
25	$-0.480+0.380i$	$-0.517+0.364i$
26	$-0.244+0.349i$	$-0.273+0.350i$
27	$-0.082+0.225i$	$-0.135+0.244i$
28	$-0.028+0.123i$	$-0.076+0.127i$
29	$-0.011+0.061i$	$-0.045+0.068i$

D. Structure of η_l in the absorption region

One of the interesting and apparently puzzling features in ^{16}O+^{28}Si scattering at $E_{\rm lab}=55$ MeV is the oscillatory structures displayed by the reflection function in the absorption region close to the orbiting partial waves. Typical cases of HIS which do not manifest large angle oscillations do not show such structures in η_l. Figure 13 clarifies this point. We offer the following explanation for this contrasting behavior of η_l as a function of l.

First we consider η_l for typical HIS, like the η_l for ^{18}O+^{58}Ni at $E_{\rm lab}=60$ MeV (Fig. 13). In a typical heavy ion collision, it is reasonable to assume that the amount of absorption generated by a given region will depend on the ratio

$$\gamma(l,k,r)=\frac{W_n(r)}{k^2-V_n(r)-V_c(r)-l(l+1)/r^2}\ , \tag{47}$$

since $W_n(r)$ is responsible for absorption and the denominator corresponds to pure scattering in the absence of $W_n(r)$. But in typical HIS one has $\eta_l \simeq \text{const} \simeq 0$ for $l \leq l_c$. Therefore one can say that η_l is *independent* of l for $l < l_c$. This implies only that domain of r is important for full absorption in which $\gamma(l,k,r)$ or $V_{\text{eff}}(l,r)$ is more or less *independent* of l. It is reasonable to expect that due to the reduced kinetic energy and hence the increased time spent by the colliding system around the barrier, maximum absorption is taking place in that region. It is found that if energy is not close to the Coulomb barrier, $\gamma(l,k,r)$ for typical HIS systems is independent of l in the neighborhood of the position of $r=R_B$ of the Coulomb barrier for $l < l_c$. This is because

$$|k^2 - V_n(r) - V_c(r)| \gg \lambda^2/r^2, \quad l < l_c, \quad r \sim R_B \ . \quad (48)$$

For example, for the $^{18}O+^{58}Ni$ system at $E_{\text{lab}}=60$ MeV shown in Fig. 13, $R_B \sim 9.74$ fm,

$$|k^2 - V_n(r) - V_c(r)| \sim 9.75 \text{ fm}^{-2}$$

at $r=R_B$. Hence the inequality (48) is quite valid for $l_c \simeq 16$. In fact, in this case $l < 20$ are more or less fully absorbed. Thus we find an interesting correlation between full absorption for $l < l_c$ and surface dominance of typical HIS.

But in the $^{16}O+^{28}Si$ case under study the situation is different. In this case

$$k^2 - V_n(r) - V_c(r) \simeq \frac{l(l+1)}{r^2} \ , \qquad l_i \leq l \leq l_f, \quad r \simeq R_B \quad (49)$$

Therefore for $l < l_i$ (but not $l \ll l_i$) the inequality (48) will not hold and hence we cannot assume $\gamma(l,k,r)$ to be more or less independent of l for $l < l_i$ in the vicinity of $l=l_i$. This means η_l in this region can be expected to show considerable variation as a function of l. Figure 13 makes this amply clear. We can conclude that if for a set of important partially absorbed partial waves in the barrier region $\text{Re}V_{\text{eff}}(l,r) \sim k^2$, $r \sim R_B$, then η_l can be expected to show some significant l dependence even for the strongly absorbed partial waves. This condition is fulfilled by the orbiting partial waves in the case of $^{16}O+^{28}Si$ at $E_{\text{lab}}=55$ MeV.

V. CONCLUDING REMARKS

From our extensive analysis of $^{16}O+^{28}Si$ scattering at $E_{\text{lab}}=55$ MeV we find that a set of three orbiting partial waves contributing to orbital amplitude $A_0(\theta)$ play a crucial role in the back angle enhanced oscillations of the scattering cross section. It is found that $A_0(\theta)$ and the background amplitude $A_b(\theta)$ act almost coherently at large angles $\theta \lesssim 180°$ and the interference between them is almost, but not completely, destructive. It is tempting to interpret the almost π phase difference between $A_0(\theta)$ and $A_b(\theta)$ at large angles as due to the "thin film effect" generated by the barrier. Let us maintain $\theta=180°$ in order to clarify this point. Outside the barrier,

$$k_{\text{eff}} = [k^2 - V_{\text{eff}}(l,r)]^{1/2}$$

is quite large as compared to k_{eff} on the barrier. Furthermore the "thickness" of the barrier (say about 0.5 fm around $r=8.5$ fm) is small compared to the de Broglie wavelength $\lambda = 2\pi/k$ in that region for the orbiting partial waves. For example, $\lambda_{\text{eff}} \simeq 19.8$ fm for $l=25$ at $r=8.4$ fm. Even in the region just outside the barrier, λ_{eff} is fairly large compared to the barrier width. Therefore the "refractive index" of the "thin" barrier region is large in comparison with the outside region. Now, using the analogy of wave optics we can conclude that $A_0(\theta)$ reflected from the interior region of the barrier will be out of phase with $A_{\text{ext}}(\theta)$ describing the scattering from the outside region. Thus we obtain a simple qualitative and interesting explanation of the origin of the almost destructive interference. We will not attempt rather involved detailed wave optic analysis of the general problem in view of the complete quantum mechanical analysis described earlier.

We find from our mathematical analysis that at large angles $\theta \lesssim 180°$, both $A_0(\theta)$ and $A_b(\theta)$ are dominated by the same Legendre polynomial. This automatically explains the similarity of the cross sections generated by the exact Regge pole amplitude and the corresponding Regge background amplitude.[2] Similarly, the same Legendre polynomial dominance in Eq. (29) explains the success of a purely parametric Regge pole model in explaining the back angle enhanced oscillations. Furthermore, in our calculations using the LC potential we find that the sequence of infinitely many Regge poles generated by the barrier region in the WKB formula for the S matrix can be correlated with the exact quantal Regge pole associated with orbiting. Similarly, the physical origin of the oscillatory structure of η_l in the absorption region is found to be correlated with the fact that $V_{\text{eff}}(l,R_B) \approx k^2$ for the set of orbiting partial waves.

One of the authors (C.S.S.) acknowledges with gratitude the discussions he had with D. M. Brink, A. Zuker, and J. Richert on the orbiting phenomena, and also the financial assistance provided by the Centre de Recherches Nucléaires, Strasbourg, France. C. S. S. also acknowledges financial assistance from the Department of Atomic Energy, Government of India, in the form of research Grant No. 37/49/80-G.

*On leave from Physics Group, Birla Institute of Technology and Science, Pilani (Raj) 333031, India.

[1]P. Braun-Munzinger, G. M. Berkowitz, T. M. Cormier, C. M. Jachcinski, J. W. Harris, J. Barrette, and M. J. Le Vine, Phys. Rev. Lett. 38, 944 (1977).

[2]T. Takemasa and T. Tamura, Phys. Rev. C 18, 1282 (1978).

[3]M. C. Mermaz, Phys. Rev. C 23, 755 (1981).

[4]F. Videback, P. R. Christensen, O. Hansen, and K. Ulbak, Nucl. Phys. A256, 301 (1976).

[5]S. Mukherjee, Phys. Rev. 160, 1546 (1967); S. Mukherjee and C. S. Shastry, *ibid.* 169, 1234 (1968); R. Shanta and C. S. Shastry, *ibid.* 176, 1254 (1968); T. Tamura and H. H. Wolter, Phys. Rev. C 6, 1976 (1972).

[6]*Handbook of Mathematical Functions* edited by M. A. Abramowitz and I. A. Stegun (Dover, New York, 1964), p. 257.

[7]See for example, C. Marty, Stony Brook report, 1978 (unpublished).

[8]*Higher Transcedental Functions,* Bateman Manuscript Project, edited by A. Erdelyi (McGraw-Hill, New York, 1953), Vol. 2, p. 149.

[9]*Higher Transcedental Functions,* Bateman Manuscript Project, edited by A. Erdelyi (McGraw-Hill, New York, 1953), Vol. 1, p. 158.

[10]J. Barrette, M. J. Le Vine, P. Braun-Munzinger, G. M. Berkowtiz, M. Gai, J. W. Harris, and C. M. Jachcinski, Phys. Rev. Lett. 40, 445 (1978).

[11]N. Cindro, Riv. del Nuovo Cimenta 4, 1 (1981).

[12]D. M. Brink and N. Takigawa, Nucl. Phys. A279, 159 (1977).

[13]D. M. Brink (private communication).